

# A new model for the $\nu_1$ vibrational band of HCN in cometary comae, with application to three comets<sup>★</sup>

M. Lippi<sup>1</sup>, G. L. Villanueva<sup>2</sup>, M. A. DiSanti<sup>2</sup>, H. Böhnhardt<sup>1</sup>, M. J. Mumma<sup>2</sup>, B. P. Bonev<sup>2,4</sup>, and D. Prrialnik<sup>3</sup>

<sup>1</sup> Max Planck Institute for Solar System Research, Katlenburg-Lindau, Germany  
e-mail: ciortellina@gmail.com

<sup>2</sup> The Goddard Center for Astrobiology, NASA Goddard Space Flight Center, Greenbelt, MD, 20771, USA

<sup>3</sup> Department of Geophysics and Planetary Sciences, Tel Aviv University, Tel Aviv, Israel

<sup>4</sup> Dept. of Physics, Catholic University of America, Washington DC, 20064, USA

Received 26 June 2012 / Accepted 28 December 2012

## ABSTRACT

**Aims.** Hydrogen cyanide (HCN) radiates effectively at infrared wavelengths in cometary atmospheres, and a new quantum-band model is needed to properly interpret high-resolution spectra. HCN spectra of comets 8P/Tuttle, C/2007 W1 (Boattini), and C/2008 Q3 (Garradd) have been recorded by our team using the high-resolution CRYogenic InfraRed Echelle Spectrometer (CRIRES) at the Very Large Telescope (VLT), ultimately posing an excellent test for our newly developed model.

**Methods.** We developed a quantum-band model for the  $\nu_1$  fundamental of HCN using the latest spectroscopic parameters available and with it retrieved HCN in the above mentioned three comets. For each comet, we sampled several lines of HCN in the spectral region near 3  $\mu\text{m}$ , and retrieved molecular production rates, mixing ratios, and rotational temperatures.

**Results.** When compared to other comets, 8P/Tuttle is relatively depleted in HCN, while C/2007 W1 (Boattini) appears to be enriched and C/2008 Q3 (Garradd) normal. The spatial profile of HCN observed in 8P/Tuttle is symmetric, consistent with isotropic outgassing from the nucleus, while in comet C/2007 W1 we observed an asymmetric excess of HCN in the anti-solar direction. We investigated the HCN-CN parentage by comparing our production rate ratios (HCN/H<sub>2</sub>O) with those of CN/OH derived at optical wavelengths. In comet C/2007 W1 the two mixing ratios are comparable, while in 8P/Tuttle our derived HCN abundance is too low to support the HCN molecule as the only parent of the CN radical.

**Key words.** molecular data – astrobiology – comets: individual: 8P/Tuttle – comets: individual: C/2007W1 (Boattini) – infrared: general – comets: individual: C/2008 Q3 (Garradd)

## 1. Introduction

Comets are considered to be among the least processed bodies of the solar system, and their compositions may reveal critical information about the diverse conditions that were present in the proto-planetary nebula, the place and the time where and when they formed. A taxonomy based on the chemical composition of these bodies could test a possible radial gradient in the chemistry of icy planetesimals in the proto-planetary disk, along with the dynamical models that predict their dissemination. As sublimating volatiles are released in cometary comae, they radiate effectively in the infrared via solar-induced fluorescence. The analysis of this emission using high-resolution spectroscopy (resolving power  $\geq 20\,000$ ) in the mid-IR (3–5  $\mu\text{m}$ ) permits the sampling of the chemical and physical properties of cometary volatiles with high sensitivity.

Today, the increasing capabilities of telescopes and instruments allow us to observe the inner part of a cometary coma with unprecedented high spatial and spectral resolution. To properly interpret these spectra, advanced molecular models that compute fluorescence emission efficiencies are necessary to convert the measured line fluxes to molecular production rates. These models require a precise description of the rotational structure

of all vibrational levels involved, together with accurate statistical weights, selection rules, perturbations (e.g. Coriolis effects, splittings, tunneling) and band-emission rates.

We present a new fluorescence model of the  $\nu_1$  ro-vibrational fundamental band of HCN and use this to retrieve production rates, mixing ratios relative to water, and rotational temperatures in three comets observed by our team at the Very Large Telescope (VLT). The model can be extended to other species to correctly interpret cometary spectra obtained using high-dispersion spectroscopy.

## 2. HCN fluorescence model

### 2.1. The importance of HCN in cometary studies

Hydrogen cyanide (HCN) is a typical component present in cometary ices that may have played an important role in the development of life on our planet. HCN could have been deposited on Earth by comets, meteorites, and interplanetary dust particles, giving rise to essential polymeric structures, and, in presence of liquid water, to formation of amino acids and proteins and ultimately to life as we know it (Matthews & Minard 2008).

Comparison of HCN abundances in comets with those observed in the interstellar medium can be used to investigate the primordial conditions of our solar system, while the relative abundance among nitrogen-bearing molecules in comets (HCN, NH<sub>3</sub>, N<sub>2</sub>, etc.) may be indicative of the formation temperature

<sup>★</sup> Based on observations obtained at the ESO – European Southern Observatory at Cerro Paranal, Chile, under programs 080.C-0257(A), 081.C-0116(A), 083.C-0646(A).

and the kind and degree of processing experienced by pre-cometary material, whether in the natal cloud or in the solar nebula (Mumma et al. 1993; Mumma & Charnley 2011).

HCN is a linear molecule with a triple bond between carbon and nitrogen, and it is characterized by three normal vibrational modes: C-H stretching, C-N stretching, and H-C-N bending. Emission lines in cometary comae related to the C-H stretching mode can be easily observed in the IR spectral region, at about 3.3  $\mu\text{m}$ .

## 2.2. The model

Currently, the increasing capability of infrared telescopes and instrumentation enables astronomical sensing with unprecedented sensitivity, and with spectral resolution sufficient to reveal the rotational structure of vibrational bands emitted by molecules in the inner cometary coma. With this higher precision, it becomes essential to employ improved fluorescence models that can fully interpret the observed spectra.

Fluorescence is a non-LTE (non local thermal equilibrium) process, and for this reason it cannot be simply described using values tabulated in terrestrial line atlases that are suitable for an LTE regime (e.g., HITRAN Rothman et al. 2009). If the goal is to correctly reproduce the observed emissions, it is fundamental to build a complete quantum mechanical model, which is more suitable to describing this physical process. Previous models for synthesizing HCN spectra (Crovisier 1987; Magee-Sauer et al. 1999; Mumma et al. 2001) are valuable tools for this analysis, and building on them we have developed a new model for HCN that incorporates the latest spectroscopic data.

First of all, our new model reproduces more reliable line-by-line fluorescence efficiencies ( $g$ -factors), beginning with the precise knowledge of the rotational structure for each vibrational level involved. Using information contained in the latest HITRAN compilation (Rothman et al. 2009), we have re-built the ro-vibrational structure of the HCN molecule and computed all other necessary parameters, including the Einstein A-coefficients for spontaneous emission. By doing so, we retain complete control of the model parameters. Moreover, with this method we are able to include the latest updated molecular band parameters (see Table 1), and to include in the computation various perturbations (e.g., Coriolis effects, level splittings, and tunneling) that were not considered in previous models.

The solar flux received by the comet is another important factor. Our previous model approximated the wavelength-dependent solar flux by a blackbody spectrum. However, the fluorescence excitation of a ro-vibrational band depends on the absolute solar flux that excites the molecule, so the approximation by a simple blackbody (Planck function) may lead to inaccurate pumping calculations. For this reason we used a more realistic solar spectrum, obtained by convolving a continuum model (Kurucz 1997) with the accurate Hase solar atlas (Hase et al. 2006), which consists of an empirical detailed line-by-line model of the solar transmittance spectrum (details of this solar model are described in Appendix B of Villanueva et al. 2011b). This solar model also takes into account the presence of Fraunhofer absorption lines in the solar spectrum, requiring the calculation of  $g$ -factors for the corresponding heliocentric velocity of the comet (Swings 1941). Omitting the Swings effect will lead to incorrect retrievals of rotational temperatures, since these are derived from measured line-by-line intensities after correcting for the solar pumping flux.

Collision partners in cometary atmospheres usually lack sufficient energy to excite vibrational transitions, and the rate of

**Table 1.** Constants used for the HCN- $\nu_1$  model.

Constant	Value	Units	Ref.
$B_{\text{low}}$	1.478221840	$\text{cm}^{-1}$	1
$D_{\text{low}}$	$2.91047 \times 10^{-6}$	$\text{cm}^{-1}$	1
$H_{\text{low}}$	$3.40 \times 10^{-12}$	$\text{cm}^{-1}$	1
$B_{\text{up}}$	1.4677983422	$\text{cm}^{-1}$	1
$D_{\text{up}}$	$2.8856236 \times 10^{-6}$	$\text{cm}^{-1}$	1
$H_{\text{up}}$	$3.6215 \times 10^{-12}$	$\text{cm}^{-1}$	1
$\nu_0$	3311.476834	$\text{cm}^{-1}$	1
$S_v$	$0.9062 \times 10^{-17}$	$\text{cm}/\text{molecule cm}^{-2}$	2
$I_a$	0.98511	(Terrestrial)	3
$h$	$6.626068 \times 10^{-34}$	J/s	4
$k$	$1.380650 \times 10^{-23}$	J/K	4
$c_2$	1.4387752	K cm	4
$c$	$2.99792458 \times 10^8$	m/s	4
$A_1$	-0.0015091	-	2

**References.** (1) Maki et al. (1996); (2) Malathy Devi et al. (2003); (3) Šimečková et al. (2006); (4) Rothman et al. (2009).

quenching collisions is much lower than radiative decay rates for (infrared-active) excited states. Thus, the vibrational manifold is not populated in LTE. Instead, solar radiation pumps the molecules into an excited vibrational state, which then de-excites by rapid radiative decay. Infrared photons are emitted through decay to the ground-vibrational state either directly (resonant fluorescence) or through branching into intermediate vibrational levels (non-resonant fluorescence). Optical pumping in the  $\nu_1$  band is the expected dominant factor in the excitation of this band in comets, and it is the sole pumping mechanism we consider here, although additional excitation cascading from levels with energies higher than  $\nu_1$  may also contribute, albeit in a minor way.

Knowledge of the initial (or equilibrium) population in the ground-vibrational state is fundamental when computing the pumping rates into individual rotational levels in the upper vibrational state of interest; since collisions dominate radiative decay in the pure rotational transitions, we can assume a rotational temperature  $T_{\text{rot}}$  to describe the rotational population (Xie & Mumma 1992).

Using the appropriate selection rules, the frequencies of the allowed transitions between the two vibrational levels involved (ground and  $\nu_1$ ) are computed as

$$\nu_J = E_{\text{up}}(J_{\text{up}}) - E_{\text{low}}(J_{\text{low}}) + \nu_0, \quad (1)$$

where  $\nu_0$  is the frequency of the pure vibrational transition, and  $E_{\text{low}}$  and  $E_{\text{up}}$  are given by

$$\begin{aligned} E_{\text{low}} &= B_{\text{low}}J(J+1) - D_{\text{low}}J^2(J+1)^2 + H_{\text{low}}J^3(J+1)^3, \\ E_{\text{up}} &= B_{\text{up}}J(J+1) - D_{\text{up}}J^2(J+1)^2 + H_{\text{up}}J^3(J+1)^3. \end{aligned} \quad (2)$$

In Eq. (2), the subscripts “low” and “up” refer to the lower and upper vibrational levels,  $B_{\text{low}}$  and  $B_{\text{up}}$  are the rotational constants,  $J$  is the rotational angular momentum quantum number (which takes integer positive numbers,  $J = 0, 1, 2$ , etc.);  $D_{\text{low}}$ ,  $D_{\text{up}}$ ,  $H_{\text{low}}$ , and  $H_{\text{up}}$  are the second and third rotational constants for the second- and third- order corrections. Values of the rotational constants and  $\nu_0$  in Eqs. (1) and (2) were derived in the laboratory by performing highly precise spectroscopic measurements of several ro-vibrational bands. See band constants and corresponding references in Table 1.

To compute the rotational line intensities, we partitioned the band intensity along the R and P branches by scaling by the corresponding Hönl-London factor  $L_J$  and the fractional population

of the lower state energy (including self-emission, see Eq. (3)). We also compensated for rotational-vibrational interactions by means of the Herman-Wallis factor  $F$ . In our model, we computed  $L_J$  using the expression  $L = m^2/|m|$ , with  $m = J(J+1)$  for the  $R$ -branch and  $m = -J$  for the  $P$ -branch, while for  $F$  we used the approximation  $F = (1 + A_1 m)^2$ , with  $m$  defined as before (for both equations see Malathy Devi et al. 2003, and references therein); the parameter  $A_1$  was measured in the laboratory and its value is listed in Table 1.

The rotational line intensities were then computed as in Malathy Devi et al. (2003):

$$S_{lu} = \frac{\nu}{\nu_0} L_J \frac{S_v}{Q_r} e^{-c_2 E_{l\text{ow}}/T_{\text{rot}}} \left[ 1 - e^{-c_2 \nu/T_{\text{rot}}} \right] F; \quad (3)$$

here,  $Q_r$  is the rotational partition function at the rotational temperature  $T_{\text{rot}}$ ,  $c_2 = hc/k$ , and  $S_v$  is the vibrational band intensity. The value for  $S_v$ , listed in Table 1, was measured in the laboratory for a standard temperature of 296 K, but it is possible to convert it to any temperature  $T$  (see for example Šimečková et al. 2006). The rotational partition function is given by

$$Q_r = \sum_J w_{\text{low}} e^{-c_2 E_{\text{low}}/T_{\text{rot}}}. \quad (4)$$

We directly computed the Einstein coefficients for spontaneous emission  $A_{ul}$  following Šimečková et al. (2006):

$$A_{ul} = \frac{8\pi c \nu^2 Q_r(T_{\text{rot}}) Q_v(T_{\text{rot}}) S_{lu}}{e^{-c_2 E_{l\text{ow}}/T_{\text{rot}}} (1 - e^{-c_2 \nu/T_{\text{rot}}}) I_a w_{\text{up}}}. \quad (5)$$

In Eq. (5),  $Q_v(T_{\text{rot}})$  is the vibrational partition function, which for simplicity was assumed to be 1,  $w_{\text{up}}$  is the degeneracy of the upper state, and  $I_a$  is the isotopic ratio for the HCN molecule (we adopted the terrestrial value, see Table 1). The Einstein coefficient for absorption  $B_{lu}$  is related to the Einstein coefficients for spontaneous emission  $A_{ul}$  by the following equation:

$$A_{ul} = 8\pi h \nu^3 B_{lu} (w_{\text{low}}/w_{\text{up}}). \quad (6)$$

If  $J_\nu$  is the solar flux received by the comet at frequency  $\nu$ , the total pumping  $g$ -factor for a ro-vibrational level  $u$  is

$$g_u = \sum_l g_{lu} = \sum_l \frac{J_\nu B_{lu} w_{\text{low}} e^{-c_2 E_{l\text{ow}}/T_{\text{rot}}}}{Q_r(T_{\text{rot}})}, \quad (7)$$

where  $w_{\text{low}}$  is the degeneracy of the lower state; for each line, we took the value for  $J_\nu$  retrieved from the adopted solar model described before.

Once all pump factors were computed, the cometary fluorescence rates, i.e., the  $g$ -factors, are given by

$$g_{ul} = g_u \frac{A_{ul}}{A_u}, \quad (8)$$

where  $A_{ul}/A_u$  represents the branching ratios for each line, with

$$A_u = \sum_l A_{ul} \quad (9)$$

as the sum of all probabilities accessing the ro-vibrational level  $u$ .

The model development is described in greater detail in Lippi (2010).

### 3. Observations and data analysis

The observations were performed using the cryogenic high-resolution infrared echelle spectrometer CRIRES at the VLT at Cerro Paranal, Chile (Käufl et al. 2004). The high resolving power achieved by this instrument (maximum resolving power  $\lambda/\Delta\lambda \approx 100\,000$  for a 0.2 arcsec slit width) allows us to resolve the rotational structure of the molecular spectra, to study the excitation temperature, and to distinguish cometary (Doppler shifted) emission lines from atmospheric features. Moreover, the VLT adaptive optics (MACAO) system permits increased spatial resolution and improves the signal-to-noise ratio in the central part of the coma.

The targets that we selected are 8P/Tuttle (hereafter, 8P), C/2007 W1 (Boattini) (hereafter, C/2007 W1), and C/2008 Q3 (Garradd) (hereafter, C/2008 Q3).

8P is a Halley-type comet with an orbital period of 13.6 years. Observations of this comet and the corresponding flux-calibration standard star (BS718) were performed in service mode near perihelion (27 January 2008, minimum heliocentric distance of 1.02 AU), spanning the UT dates 26–29 January 2008 (see Böhnhardt et al. 2008).

C/2007 W1 is a dynamically new comet<sup>1</sup> that entered the inner solar system in 2008. Our first observing run covered the period from 11 May 2008 to 30 May 2008, before perihelion (0.85 AU, on 24 June 2008), while the second was performed during the first week of July 2008. Different settings for C/2007 W1 and the corresponding standard star (BS740) were sampled in service mode during the night between 30 and 31 May 2008.

C/2008 Q3 is a dynamically new comet<sup>1</sup> that reached perihelion (1.80 AU) on 23 June 2009. Our observations of C/2008 Q3 and the corresponding flux-calibration standard star (BS8204) were performed in visitor mode, spanning the UT dates 6–8 June 2009.

We used several instrument settings between  $\approx 2.8$  and  $4.7 \mu\text{m}$  for the detection of various species in the coma. To sample HCN we centered the instrument setting near  $3 \mu\text{m}$ , adjusting it slightly for each comet based on its geocentric velocity, to optimize the sampling of the strongest HCN lines. We used the 0.4 arcsec slit width, which delivers a resolving power of 50 000, and locked the AO system on the central brightness condensation of the coma, effectively reducing slit losses. The telescope was nodded along the slit in an ABBA sequence and “jittered” along the slit by adding a small random (but well-known) offset around the nominal A and B positions to minimize the effect of bad pixels on the detector array. In Table 2 we report the ephemeris for the three comets and summarize the conditions and parameters for each observing night.

The echellograms were processed using custom algorithms tailored for CRIRES (including jitter corrections); these are based on well-tested data reduction and analysis routines developed for the NIRSPEC and CSHELL instruments (Villanueva et al. 2008; DiSanti et al. 2001). First-order processing of the data included sky-subtraction, flat-fielding, removal of high dark current pixels and cosmic ray hits; data were then spatially and spectrally registered. Frequency calibration and correction for telluric absorption used synthetic transmittance spectra based on rigorous line-by-line, layer-by-layer radiative transfer modeling of the terrestrial atmosphere, using LBLRTM (Villanueva et al. 2011b; Clough et al. 2005). For each setting, a modeled continuum for the dust affected by atmospheric transmittance was

<sup>1</sup> See Nakano notes NK 1656 and NK 1886 at <http://www.oaa.gr.jp/~oacacs/nk.htm>



**Table 2.** Ephemeris and observing parameters for the observed comets.

Comet	Date (UT)	Start (UT)	End (UT)	$R_h$ AU	$dR_h/dt$ $\text{km s}^{-1}$	$\Delta$ AU	$d\Delta/dt$ $\text{km s}^{-1}$	Air mass	Seeing ( $''$ )	$\lambda$ range $\text{cm}^{-1}$
8P	27 Jan. 08	01:27:58	02:06:04	1.03	0.80	0.54	24.71	1.4	0.7	3345.4–3259.9
C/2007 W1	30 May 08	23:14:34	23:36:02	0.97	−15.27	0.24	−7.04	1.3	0.8	3332.6–3263.9
C/2008 Q3	8 Jun. 09	00:16:59	01:02:16	1.81	−2.49	0.95	11.68	1.1	0.8	3344.1–3273.9

**Notes.**  $R_h$  and  $\Delta$  are the heliocentric and geocentric distances respectively, while  $dR_h/dt$  and  $d\Delta/dt$  are the comet-Sun and the comet-Earth relative velocity, respectively. For all observations we used a nodding value of  $\pm 15''$ , a jittering value of  $\pm 5''$ , a  $0.4''$  slit width, and 60 s integration time.

subtracted from the cometary spectrum, thereby isolating the molecular emission lines.

The calibrated echellograms were ultimately combined and cometary spectra were extracted by spatially summing the signal contained in 15 rows ( $1.3''$ ) centered on the peak continuum emission. With the adopted  $0.4''$  slit, our field-of-view (FOV,  $0.4'' \times 1.3''$ ) centered on the comet nucleus was  $157 \times 509 \text{ km}^2$  for 8P,  $69 \times 226 \text{ km}^2$  for C/2007 W1, and  $276 \times 896 \text{ km}^2$  for C/2008 Q3.

Figure 3 shows a selection of the echellograms obtained for the different observations, coupled with the corresponding extracted spectra (in each plot, the red lines in the upper spectrum represent the  $\pm 1\sigma$  confidence limits).

## 4. Results and discussion

### 4.1. Rotational temperatures

To determine the total production rates from individual line intensities it is fundamental to know the optimal value for the rotational temperature  $T_{\text{rot}}$ , since it describes the population distribution among the rotational energy levels in the ground-vibrational state. Conversely, the temperature dependence of the  $g$ -factors for individual ro-vibrational lines is needed to obtain an effective rotational temperature from the measured line intensities. The more accurate the determination of  $T_{\text{rot}}$ , the more reliable the retrieved production rates from measured line intensities.

We derived line-by-line column densities by dividing the measured line fluxes by the calculated (temperature-dependent) individual  $g$ -factors computed by our model, after correcting for atmospheric transmittance. We assumed that a single rotational temperature ( $T_{\text{rot}}$ ) characterizes the populations in rotational levels of the ground vibrational state, and calculated the  $g$ -factors for a sequence of temperatures. At the correct rotational temperature, the quantity  $F/(g(T_{\text{rot}}))$  should be independent of the lower state energy ( $E_{\text{low}}$ ) and should agree for all sampled lines (see Dello Russo et al. 2004). Thus, we can produce rotation diagrams ( $F/(g(T_{\text{rot}}))$  vs.  $E_{\text{low}}$ ) at individual assumed temperatures. At the optimum value of  $T_{\text{rot}}$ , the linear least-squares polynomial fit to  $F/(g(T_{\text{rot}}))$  vs.  $E_{\text{low}}$  has a slope of zero. This process thereby provides the best value for  $T_{\text{rot}}$ , and also its relative confidence limits ( $\pm 1\sigma$  uncertainty – for additional details, see Bonev et al. 2013; DiSanti et al. 2006, 2001; Lippi 2010; Bonev 2005). The retrieved rotational temperature is most accurate when a wide range of rotational energies is sampled.

Using this method, and considering optical-depth effects negligible for the HCN emission lines in the observed regions, a rotational temperature of  $(53 \pm 2) \text{ K}$  was retrieved for comet 8P/Tuttle, in agreement with the rotational temperature obtained for water ( $60_{-9}^{+8} \text{ K}$ ), observed during the same observing run (Bönnhardt et al. 2008); this value is comparable with the one

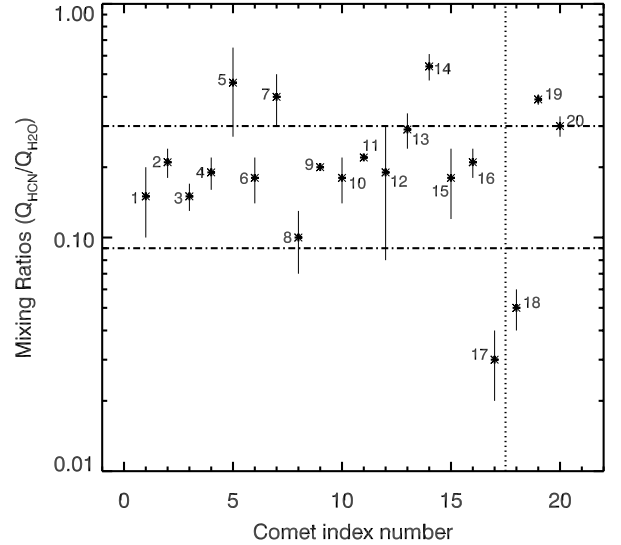


**Fig. 1.** Comparison of HCN content measured in the IR, among different comets. The dashed-dotted lines separate HCN depleted, HCN normal, and HCN enriched comets, while the dotted vertical line separate comets reported elsewhere (*left*) from those reported in this paper (*right*). The comets in the plot are 1. C/2004 Q2, 2. C/1999 H1, 3. C/2000 WM1, 4. C/2006 P1, 5. C/2001 A2, 6. C/1996 B2, 7. C/1995 O1, 8. C/1999 S4, 9. 1P/Halley, 10. 153P/Ikeya-Zhang, 11. 21P/Giacobini – Zinner (upper limit), 12. 73P/Schwassmann-Wachmann – Fragment C, 13. 73P Schwassmann-Wachmann – Fragment B, 14. 17P/Holmes (outburst), 15. 9P/Tempel 1 (pre impact), 16. 9P/Tempel 1 (post impact), 17. 6P/D’Arrest, 18. 8P/Tuttle, 19. C/2007 W1, 20. C/2008 Q3; (see Lippi 2010 and references therein).

of  $(54 \pm 9) \text{ K}$  reported in Kobayashi et al. (2010) and with the one of  $(51 \pm 10) \text{ K}$  reported in Bonev et al. (2008).

The retrieved rotational temperature for HCN in comet C/2007 W1 was  $66_{-7}^{+10} \text{ K}$ ; this temperature is lower than the one measured for the same comet in July 2008 ( $(84 \pm 5) \text{ K}$  reported in Villanueva et al. 2011a), and the difference can be related to the different conditions of the comet (pre-/post perihelion, different distance from the Sun, etc.) on the different observing dates.

Regarding comet C/2008 Q3, the retrieved rotational temperature was poorly determined since the frames were characterized by high noise and the number of the useful (not blended) lines was small; in this case, a fixed value of 60 K was chosen for all computations.

In Fig. 2 we show the best rotational temperature diagrams obtained for 8P and C/2007 W1.

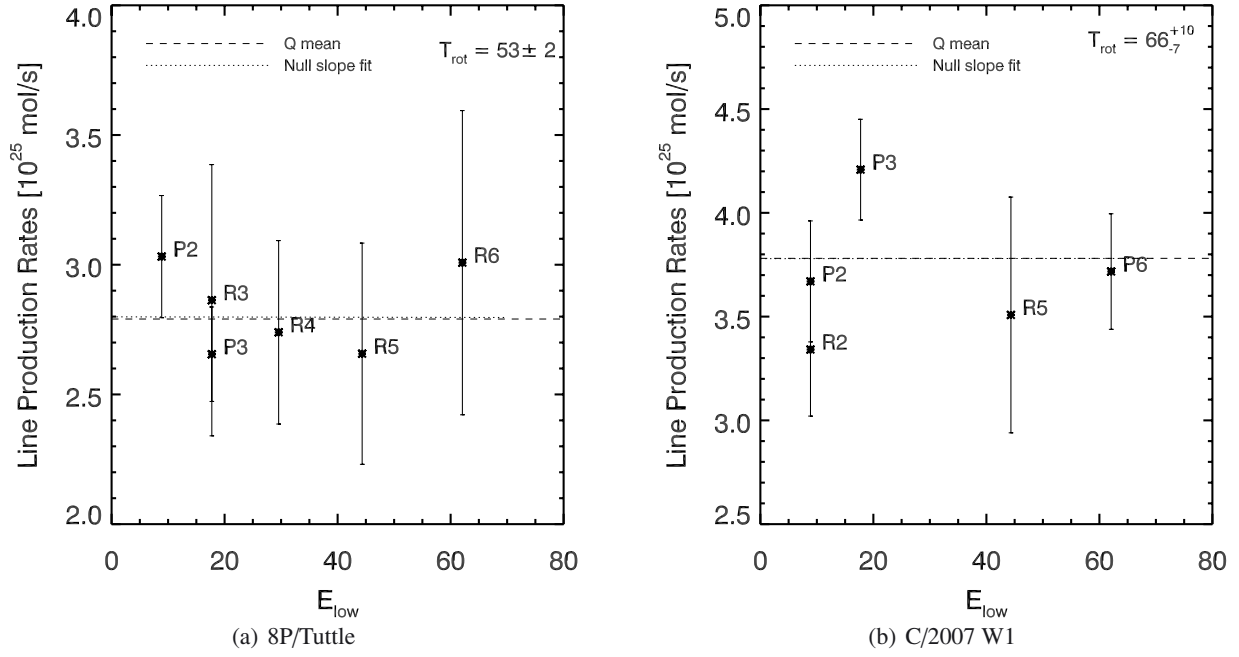


**Fig. 2.** Rotational temperature diagram for 8P/Tuttle (a) and C/2007 W1 (b). In each plot, the dashed line represents the weighted mean production rate, while the dotted line represents the “null slope” fit; individual lines are labeled with the lower level transition; error bars are plotted with vertical lines. The “null slope” rotational temperature and confidence limits are shown at top right in each panel.

#### 4.2. Production rates and mixing ratios

For each identified line, the HCN molecular production rates  $Q_i$  were retrieved through the relation

$$Q_i = \frac{4\pi\Delta^2 F_i}{g_i h\nu f(x)\tau \text{trans}(\nu, \nu_\Delta)}, \quad (10)$$

where  $\Delta$  is the geocentric distance (m),  $F_i$  (Watt/m<sup>2</sup>) is the line flux measured in a  $5 \times 15$  pixels box centered on the nucleus,  $g_i$  is the emission fluorescence  $g$ -factors (at heliocentric distance  $R_h = 1$  AU),  $h\nu$  is the energy (Joules) of a photon with wavenumber  $\nu$  (cm<sup>-1</sup>),  $\text{trans}$  is the atmospheric transmittance at the Doppler shifted frequency of the  $i$ th line at the cometary geocentric velocity ( $\nu_\Delta$ ),  $f(x)$  is the fraction of the total coma content of the targeted species sampled by the beam (see appendix in Hoban et al. 1991, for details), and  $\tau$  is the molecular photodissociation lifetime at heliocentric distance of 1 AU (we used a value of  $6.67 \times 10^4$  s, see Magee-Sauer et al. 1999, and references therein).

Since the observed beam corresponds to a small spatial coverage of the coma, the product  $f(x)\tau$  is proportional to the inverse of the gas outflow velocity  $v_{\text{gas}}$ ; if we adopt a spherical outflow model with  $v_{\text{gas}} \propto 0.8 R_h^{-0.5}$  km s<sup>-1</sup>, where  $R_h$  is in AU, we can assume the derived production rate not to be very sensitive to the assumed lifetime.

To compensate for slit-losses we calculated the growth-factor as

$$GF = \frac{Q_{\text{term}}}{Q_{\text{nc}}}, \quad (11)$$

where  $Q_{\text{nc}}$  is the nucleus-centered production rate, determined from the mean of production rates derived from individual lines weighted inversely by their own stochastic error (squared), while  $Q_{\text{term}}$  is the terminal value reached at distances beyond the slit-loss region, computed by taking the mean value of production

**Table 3.** Retrieved production rates  $Q$ , mixing ratios M.R., and HCN rotational temperatures  $T_{\text{rot}}$  for the observed comets.

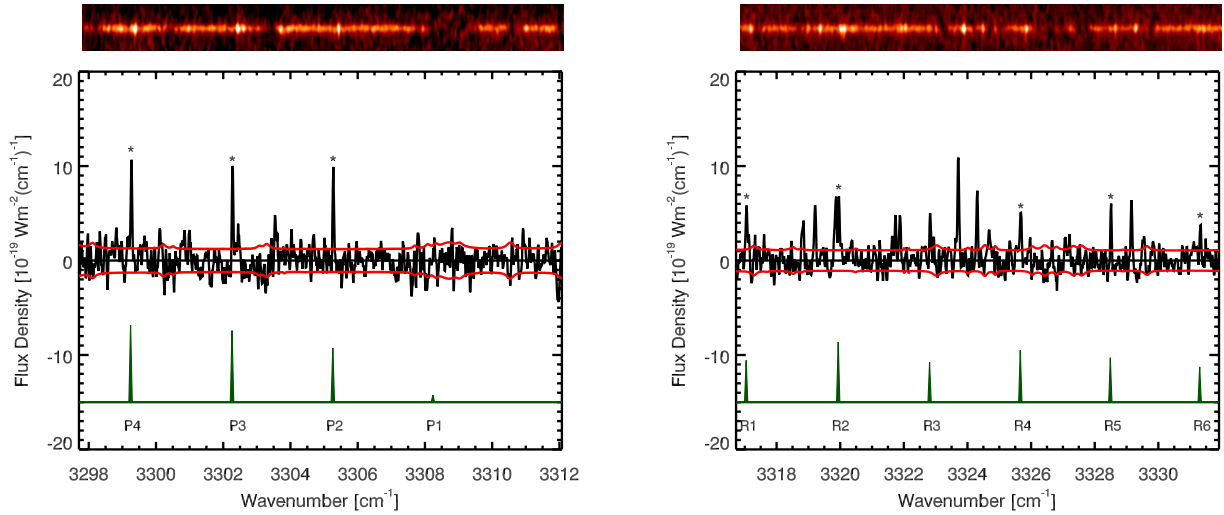
Comet	$Q_{\text{HCN}}$ 10 <sup>26</sup> (mol/s)	$Q_{\text{H}_2\text{O}}$ 10 <sup>26</sup> (mol/s)	M.R. (%) HCN/H <sub>2</sub> O	$T_{\text{rot}}$ (K)
8P	$0.28 \pm 0.03$	$570.5 \pm 38.0^{(1)}$	$0.05 \pm 0.01$	$53^{+2}_{-2}$
C/2007 W1	$0.38 \pm 0.02$	$96.5 \pm 2.8^{(2)}$	$0.39 \pm 0.02$	$66^{+10}_{-7}$
C/2008 Q3	$0.69 \pm 0.08$	$230.0 \pm 50^{(3)}$	$0.30 \pm 0.03$	60

**Notes.** Water production rates are taken from (1) Mean value in Böhnhardt et al. (2008), measured on Jan. 27, 2008; (2) DiSanti, priv. comm., measured between 30 and 31 May 2008, immediately following HCN; (3) Hartogh et al. (2010), measured on July 20, 2009, when the comet was at 1.83 AU from the Sun (we assume the water production rate to be symmetric with respect to perihelion).

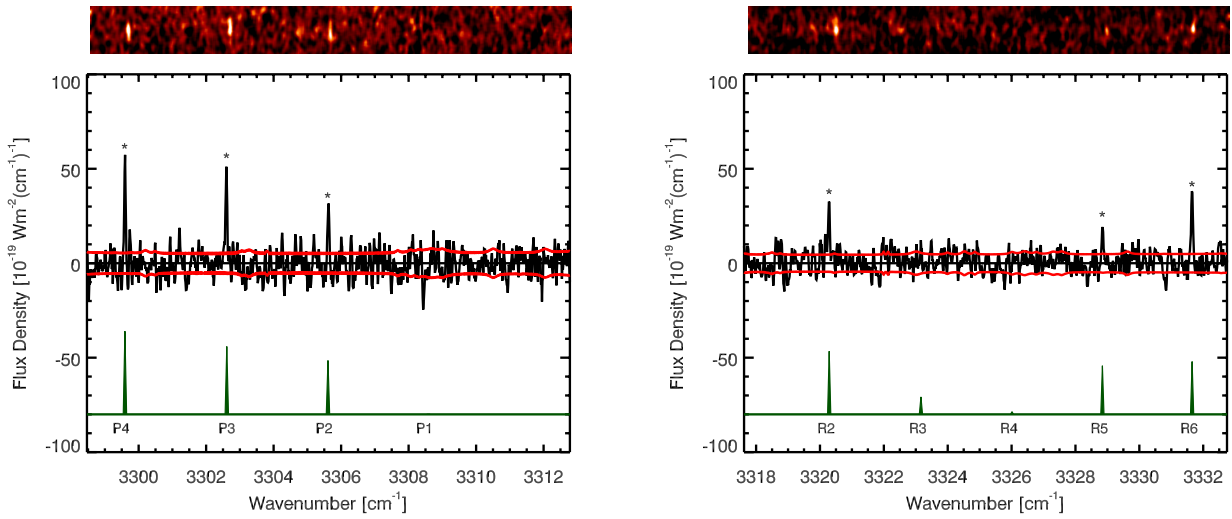
rates extracted at positions equidistant from the nucleus, along the spatial profile (see Xie & Mumma 1996; Dello Russo et al. 1998; Bonev 2005).

HCN emission lines were identified in the measured spectra at their expected Doppler-shifted positions (Table 5, rest-line frequencies were calculated using the method described in 2.2). HCN production rates, mixing ratios relative to water (in percent) and rotational temperatures obtained from these data are listed in Table 3; in the same table H<sub>2</sub>O production rates (needed to retrieve HCN/H<sub>2</sub>O mixing ratios) are indicated, with the respective references.

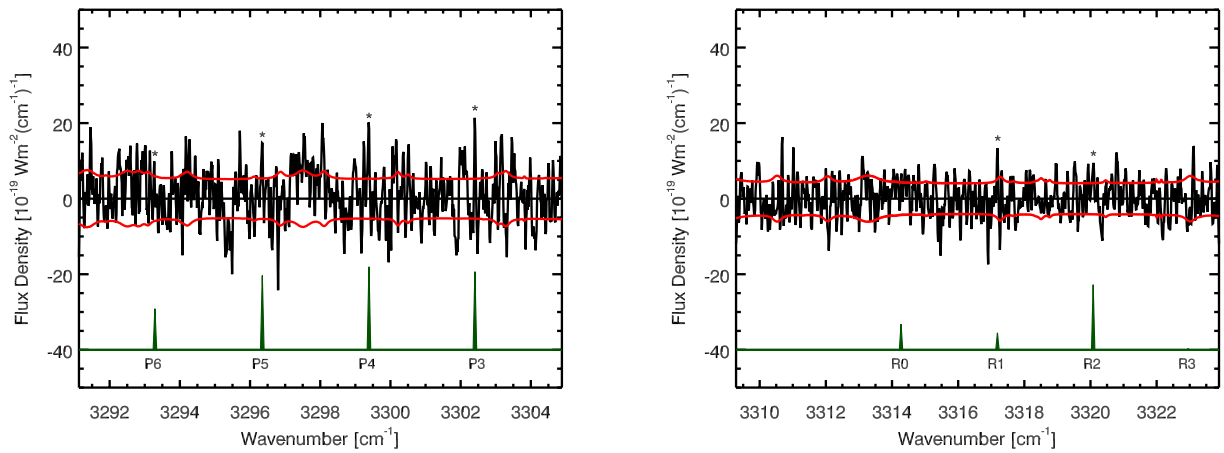
For 8P, the HCN setting spanned 3345.39 to 3259.90 cm<sup>-1</sup>, allowing us to sample eleven emission lines (see Table 5a); in our analysis, we only considered lines that were not blended with emissions from other species. We retrieved a production rate of  $(0.28 \pm 0.03) \times 10^{26}$  mol/s, and a mixing ratio (relative to water) of  $(0.05 \pm 0.01)\%$  (Böhnhardt et al. 2008 presented our results for H<sub>2</sub>O and other molecules observed on this night). Our mixing ratio for HCN on UT 27 January 2008 agrees



(a) 8P/Tuttle



(b) C/2007 W1



(c) C/2008 Q3

**Fig. 3.** Detection of HCN in the observed comets. For each spectrum the red line represents the  $\pm 1\sigma$  error. The model, Doppler-shifted and affected by transmittance, is plotted below the observed spectra; identified lines are indicated with a star. For comet C/2008 Q3 we omitted the echellograms, since they were too noisy to clearly distinguish the HCN emission lines.

**Table 4.** Comparison with other comets.

Comet	M.R. (%)
Oort cloud	0.10–0.46
Halley type	0.18–0.20
Jupiter family	0.03–0.29
8P/Tuttle	$0.05 \pm 0.01$
C/2007 W1	$0.39 \pm 0.02$
C/2008 Q3	$0.30 \pm 0.03$

**Notes.** In the first three lines of this table, we report the range of values for HCN, measured in the IR, for different dynamical types of comets. (The values are taken from Lippi 2010, and references therein).

(within  $1\sigma$  confidence limits) with values obtained on the following night ( $0.07 \pm 0.02$ ) with CRILES (UT 28 January 2008, Kobayashi et al. 2010), and on UT 22–23 December 2007 using NIRSPEC ( $0.07 \pm 0.01$ , Bonev et al. 2008).

In comet C/2007 W1, we detected ten emission lines in the spectral region  $3332.64\text{--}3263.98\text{ cm}^{-1}$  (see Table 5b) and retrieved a production rate of  $(0.38 \pm 0.02) \times 10^{26}$  mol/s, which corresponds to a mixing ratio relative to water of  $(0.39 \pm 0.02)\%$ . This value is lower than that  $(0.50 \pm 0.01)\%$  presented in Villanueva et al. (2011a). However, these authors suggested a correction of the mixing ratio for apolar species due to the possible existence of an extended source of water: in this case the HCN content would be lower, which would bring it more in line with our measurement.

HCN in comet C/2008 Q3 was measured on June 8, 2009, and even though the data were noisier than the other two datasets, we were able to identify seven emission lines between  $3344.10$  and  $3273.98\text{ cm}^{-1}$  (see Table 5c) and to retrieve a production rate of  $(0.69 \pm 0.08) \times 10^{26}$  mol/s, which translates into a mixing ratio relative to water of  $(0.30 \pm 0.03)\%$ .

Comparing the abundance ratios (HCN/H<sub>2</sub>O) measured among different comets (see Table 4 and Fig. 1), we note that HCN (0.05%) in 8P is much lower than in the other comets, except for 6P/d’Arrest (0.03%). By contrast, the HCN content in C/2007 W1 (0.39%) is comparable to that of comet C/1995 O1 (0.40%), while comet C/2008 Q3 shows 0.30%, similar to that of 73P Schwassmann-Wachmann 3 – Fragment B. In terms of the classification in Mumma et al. (2003) and DiSanti & Mumma (2008), we conclude that C/2007 W1 is HCN-enriched, while 8P is depleted in this species.

#### 4.3. Spatial profiles

The spatial profiles for molecular or continuum emissions along the slit can be used to determine the origin and outgassing of material in cometary comae. If volatiles are released solely and uniformly from the nucleus and flow outward with constant velocity, their intensity distribution along the spatial direction is expected to scale as  $1/\rho$ , with  $\rho$  being the projected distance from the nucleus. For species that are emitted from small ice grains in the coma (distributed sources) the intensity will instead fall off more slowly than  $1/\rho$ . However, it is important to notice that other properties of the comet (e.g., outflow asymmetries) and observing conditions (primarily seeing and tracking errors) may cause a deviation from the  $1/\rho$  dependence, even in the absence of a distributed source.

We obtained the spatial profile for 8P and C/2007 W1 by adding the single-line spatial profiles observed in our spectra; the

results are shown in Fig. 4; for comet C/2008 Q3 the number of the useful (bright and not blended) lines was too small to retrieve a good spatial profile.

The two comets present symmetric profiles that scale approximately like  $1/\rho$ . Comet 8P shows a small excess in the solar direction, which can be interpreted as a higher activity of the comet on the day-side with respect to the night-side. In contrast, the C/2007 W1 profile shows an excess in the anti-solar direction that could be interpreted as an indication of localized enhanced activity either coming as HCN directly from the nucleus (jets), or produced by dust grains or icy grains coming from the nucleus. C/2007 W1 was also observed in July 2008 by Villanueva et al. (2011a), displaying spatial profiles that are symmetric for HCN (and C<sub>2</sub>H<sub>6</sub>), and quite asymmetric for polar molecules (e.g., H<sub>2</sub>O and CH<sub>3</sub>OH). These asymmetries are much more pronounced than the one we saw for HCN in May 2008, and it is possible that the small asymmetry we detected is more related to the dissimilar conditions during the two observations (pre-/post perihelion, geo and heliocentric distances, integrating field of views, etc.) than to an effective HCN activity on the comet.

Since for 8P/Tuttle the dust signal was particularly strong, it was possible to compare the spatial profile of dust with that of HCN (Fig. 4a); the dust profile is also symmetric and shows a  $1/\rho$  dependence.

#### 4.4. HCN and CN production rates

Although CN has been easily observed in the visible spectral range since the earliest days of cometary spectroscopy, its origin is still only poorly understood. One of the candidate primary molecules is HCN, but direct comparisons show an inconsistency for this hypothesis; in these cases CN is thought to come partially from the dust grains present in the coma (Fray et al. 2005).

For comet 8P/Tuttle the CN radical was measured in the beginning of Dec. 2007 by Schleicher using narrow-band photometry (Schleicher & Woodney 2007); at which time, the comet was 1.30 AU from the Sun. The reported production rates for CN ( $\approx 1.66 \times 10^{25}$  mol/s) and OH ( $\approx 759 \times 10^{25}$  mol/s) imply a mixing ratio CN/OH of 0.22% in this comet. Thus, our derived mixing ratio for HCN in 8P ( $0.05 \pm 0.01\%$ ) is too low to support HCN as the only parent of the CN radical; this agrees with the result presented in Jehin et al. (2009), who provided simultaneous observations of HCN and CN, and with both Bonev et al. (2008) and Kobayashi et al. (2010), who made similar comparisons and reached the same conclusion.

Narrow-band photometry of comet C/2007 W1, observed on 30–31 July 2008, give the following results: OH production rate  $\approx 6.16 \times 10^{27}$  mol/s, CN production rate  $\approx 2.34 \times 10^{25}$ , C<sub>2</sub> production rate  $\approx 4.04 \times 10^{25}$  (Schleicher 2008). In that period the comet was at 1.07 AU from the Sun. If we scale our retrieved production rate for HCN ( $0.38 \times 10^{26}$  mol/s, for  $r_h = 0.97$  AU), we obtain a production rate of  $\approx (3.1 \pm 0.3) \times 10^{25}$  mol/s; unlike in the case of 8P/Tuttle, this result would be consistent with HCN being the only primary species of CN.

Regarding comet C/2008 Q3, no measurements for CN have been found in the literature.

The different correlation that we found for HCN and CN in comets 8P and C/2007 W1 may depend on different compositional properties of comets and/or on different processes that can be present in the coma. In particular, these two comets have shown a different behavior regarding dust production rates: comet 8P showed in our spectra a higher dust continuum signal than did comet C/2007 W1: it is then possible that, for comet



**Table 5.** Identified HCN emission lines for the three comets.

(a) 8P/Tuttle						
Line flux $10^{-20} \text{ W m}^{-2}$	$\nu$ $\text{cm}^{-1}$	$\nu_D$ $\text{cm}^{-1}$	Transition	$g$ factor $10^{-5} \text{ ph/s/mol}$	$Q_{\text{line}}$ $10^{25} \text{ mol/s}$	Transmittance
$4.65 \pm 0.91$	3331.58	3331.32	R6	1.09	$3.01 \pm 0.59$	0.97
$5.85 \pm 0.94$	3328.77	3328.52	R5	1.56	$2.66 \pm 0.43$	0.94
$7.95 \pm 1.03$	3325.94	3325.68	R4	2.05	$2.74 \pm 0.35$	0.88
$9.60 \pm 1.75$	3323.09	3322.82	R3	2.37	$2.86 \pm 0.52$	0.60
$8.84 \pm 0.89$	3320.22	3319.96	R2	2.41	$2.60 \pm 0.26$	0.97
$9.31 \pm 1.15$	3317.33	3317.07	R1-B	2.01	$3.29 \pm 0.41$	0.83
$9.90 \pm 0.77$	3305.54	3305.27	P2	2.32	$3.03 \pm 0.23$	0.97
$11.23 \pm 0.77$	3302.55	3302.28	P3	3.01	$2.66 \pm 0.18$	0.96
$12.39 \pm 0.83$	3299.53	3299.26	P4-B	3.22	$2.74 \pm 0.18$	0.93
$6.46 \pm 0.73$	3290.35	3290.09	P7-B	1.82	$2.54 \pm 0.30$	0.91
$4.47 \pm 0.66$	3287.25	3286.98	P8-B	1.25	$2.56 \pm 0.38$	0.95

(b) C/2007 W1 (Boattini)						
Line flux $10^{-20} \text{ W m}^{-2}$	$\nu$ $\text{cm}^{-1}$	$\nu_D$ $\text{cm}^{-1}$	Transition	$g$ factor $10^{-5} \text{ ph/s/mol}$	$Q_{\text{line}}$ $10^{25} \text{ mol/s}$	Transmittance
$27.80 \pm 2.14$	3331.58	3331.66	R6-B?	1.31	$7.41 \pm 0.57$	0.94
$16.98 \pm 2.75$	3328.77	3328.85	R5	1.69	$3.51 \pm 0.57$	0.74
$16.85 \pm 9.28$	3323.09	3323.17	R3	2.24	$2.63 \pm 0.14$	0.23
$20.42 \pm 1.96$	3320.22	3320.31	R2	2.14	$3.34 \pm 0.32$	0.93
$20.14 \pm 1.60$	3305.54	3305.63	P2	1.93	$3.67 \pm 0.29$	0.94
$30.55 \pm 1.76$	3302.55	3302.64	P3	2.55	$4.21 \pm 0.24$	0.87
$25.16 \pm 1.68$	3299.53	3299.61	P4-B	2.85	$3.11 \pm 0.21$	0.92
$26.06 \pm 1.95$	3293.43	3293.52	P6	2.47	$3.72 \pm 0.28$	0.73
$25.99 \pm 1.66$	3290.35	3290.44	P7-B	1.97	$4.66 \pm 0.30$	0.72
$13.40 \pm 1.44$	3287.25	3287.34	P8-B	1.49	$3.17 \pm 0.34$	0.91

(c) C/2008 Q3 (Garradd)						
Line flux $10^{-20} \text{ W m}^{-2}$	$\nu$ $\text{cm}^{-1}$	$\nu_D$ $\text{cm}^{-1}$	Transition	$g$ factor $10^{-5} \text{ ph/s/mol}$	$Q_{\text{line}}$ $10^{25} \text{ mol/s}$	Transmittance
$3.49 \pm 1.65$	3331.58	3331.46	R6	1.20	$7.66 \pm 3.61$	0.96
$5.17 \pm 1.54$	3320.22	3320.09	R2	2.28	$5.98 \pm 1.79$	0.95
$16.83 \pm 7.69$	3317.33	3317.20	R1-B	2.42	$18.37 \pm 8.40$	0.24
$8.44 \pm 1.35$	3302.55	3302.41	P3	2.79	$8.04 \pm 1.29$	0.94
$9.92 \pm 1.38$	3299.53	3299.39	P4-B	3.64	$7.24 \pm 1.01$	0.91
$6.94 \pm 1.48$	3296.49	3296.36	P5	2.89	$6.39 \pm 1.36$	0.85
$5.58 \pm 2.48$	3293.43	3293.30	P6	2.48	$5.98 \pm 2.66$	0.55

**Notes.** For each transition (indicated in the fourth column) we listed the wavenumber  $\nu$ , the Doppler shifted wavenumber  $\nu_D$  and the corresponding measured flux (at the top of the atmosphere). Modeled line  $g$ -factors at 1 AU from the Sun and retrieved line production rates  $Q_{\text{line}}$ , with the relative errors, are given in the fifth and sixth columns respectively. In the last column the values of the terrestrial atmospheric transmittance are shown. Values of  $g$ -factors are given for the “null slope” rotational temperatures of 53 K for 8P, and 66 K for C/2007 W1. With confidence limits, the retrieved values are  $53 \pm 2$  K and  $66^{+10}_7$  K, respectively. We assumed  $T_{\text{rot}} = 60$  K for C/2008 Q3. The B letter in the fourth column indicates if a detected HCN emission line is blended with emission lines coming from other molecules; for comet C/2007 W1 the line production rate relative to the R6 transition was much different from the other values (could it be that this line is blended with a line from an unknown species) and thus was not considered in the computation of production rate and rotational temperature.

C/2007 W1, CN was produced only from photolysis of HCN, while in comet 8P/Tuttle this radical was also released from dust grains in the coma.

## 5. Summary and conclusions

Comets are believed to be the remnants of solar system formation and as such they can provide unique information regarding the chemical and physical conditions in the region where they formed. High-resolution spectroscopy is fundamental for retrieving the volatile composition of cometary nuclei and for testing their nature and role in the solar system; in this scenario, HCN is

a cometary primary molecule that plays an important role, since it is considered a candidate for the development of life on Earth.

We reported HCN production rates, mixing ratios relative to water (in percent), and rotational temperatures that we retrieved for three comets: 8P/Tuttle, C/2007 W1 (Boattini), and C/2008 Q3 (Garradd). To that end, we developed a new fluorescence model for  $\nu_1$  of HCN, which calculates fluorescence efficiencies using the latest spectroscopic parameters and includes several effects (torsional Coriolis interactions, torsional splittings, Herman-Wallis effects, resonance mixing, etc.) that are often excluded in the computation of cometary  $g$ -factors; moreover, our calculation corrects the  $g$ -factors for the Swings effect and uses a



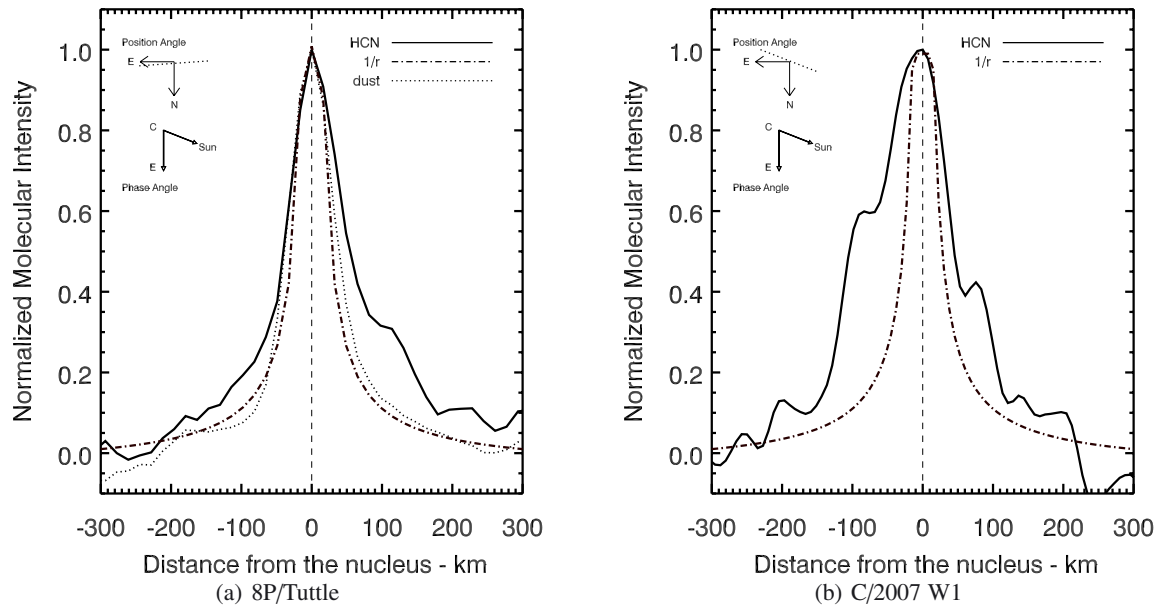


**Fig. 4.** Spatial profiles for 8P/Tuttle (a) and C/2007 W1 (b). In each plot, the HCN profile (continuum line) is compared with a  $1/\rho$  profile (dash-dotted line). The direction of the Sun is also indicated.

more realistic solar spectrum, obtained by combining empirical and theoretical data.

The observed comets displayed considerable differences, with comet 8P (a Halley-type comet) containing a very low abundance of HCN with respect to comets C/2007 W1 and C/2008 Q3, both classified as dynamically new comets. As shown in Table 4, Oort Cloud comets appear to show higher HCN abundances than Halley-type and Jupiter-family comets; in this limited sample of comets, the enrichment of HCN observed in comets C/2007 W1 and C/2008 Q3 and its depletion in 8P is consistent with this grouping.

We analyzed the spatial intensity distribution of HCN for comet 8P and C/2007 W1, finding quite symmetric profiles, suggesting that HCN is released at (or very close to) the nucleus for all these comets.

Finally, for comets 8P and C/2007 W1, we compared production rates of the primary molecule HCN with the product species CN to check a possible correlation between them: while in comet C/2007 W1 the mixing ratios of the two molecules are comparable, in 8P the abundance of HCN is not sufficient to explain the CN production in the comet, and more investigations are needed to find other possible primary candidates for this molecule.

**Acknowledgements.** We thank the VLT science operations team of the European Southern Observatory for efficient execution of the observations. This work was supported by the International Max Planck Research School, NASA's Planetary Astronomy Program, Astrobiology Program and Postdoctoral Program and the German-Israeli Foundation for Scientific Research and Development.

## References

Bönnhardt, H., Mumma, M. J., Villanueva, G. L., et al. 2008, *ApJ*, 683, L71  
 Bonev, B. P. 2005, Ph.D. Thesis, The University of Toledo  
 Bonev, B. P., Mumma, M. J., Radeva, Y. L., et al. 2008, *ApJ*, 680, L61  
 Bonev, B. P., Villanueva, G. L., Paganini, L., et al. 2013, *Icarus*, 222, 740  
 Clough, S. A., Shephard, M. W., Mlawer, E. J., et al. 2005, *J. Quant. Spectr. Radiat. Transf.*, 91, 233  
 Crovisier, J. 1987, *A&A*, 68, 223  
 Dello Russo, N., DiSanti, M. A., Mumma, M. J., Magee-Sauer, K., & Rettig, T. W. 1998, *Icarus*, 135, 377

Dello Russo, N., DiSanti, M. A., Magee-Sauer, K., et al. 2004, *Icarus*, 168, 186  
 DiSanti, M. A., & Mumma, M. J. 2008, *Space Sci. Rev.*, 138, 127  
 DiSanti, M. A., Mumma, M. J., Dello Russo, N., & Magee-Sauer, K. 2001, *Icarus*, 153, 361  
 DiSanti, M. A., Bonev, B. P., Magee-Sauer, K., et al. 2006, *ApJ*, 650, 470  
 Fray, N., Bénilan, Y., Cottin, H., Gazeau, M.-C., & Crovisier, J. 2005, *Planet. Space Sci.*, 53, 1243  
 Hartogh, P., Crovisier, J., de Val-Borro, M., et al. 2010, *A&A*, 518, L150  
 Hase, F., Demoulin, P., Sauval, A., et al. 2006, *J. Quant. Spectr. Radiat. Transf.*, 102, 450  
 Hoban, S., Mumma, M., Reuter, D. C., et al. 1991, *Icarus*, 93, 122  
 Jehin, E., Bockelée-Morvan, D., Dello Russo, N., et al. 2009, *Earth Moon and Planets*, 105, 343  
 Käufel, H., Ballester, P., Biereichel, P., et al. 2004, in *SPIE Conf. Ser.* 5492, eds. A. F. M. Moorwood, & M. Iye, 1218  
 Kobayashi, H., Bockelée-Morvan, D., Kawakita, H., et al. 2010, *A&A*, 509, A80  
 Kurucz, R. L. 1997, in *IAU Symp.* 189, eds. T. R. Bedding, A. J. Booth, & J. Davis, 217  
 Lippi. 2010, Ph.D. Thesis, Technische Universität Braunschweig, Germany (UNI-Ed.)  
 Magee-Sauer, K., Mumma, M. J., DiSanti, M. A., Russo, N. D., & Rettig, T. W. 1999, *Icarus*, 142, 498  
 Maki, A., Quapp, W., Klee, S., Mellau, G. C., & Sieghard, A. 1996, *J. Mol. Spectrosc.*, 180, 323  
 Malathy Devi, V., Benner, D., Smith, M., et al. 2003, *JQSRT*, 82, 319  
 Matthews, C. N., & Minard, R. D. 2008, in *IAU Symp.* 251, eds. S. Kwok, & S. Sandford, 453  
 Mumma, M. J., & Charnley, S. B. 2011, *ARA&A*, 49, 471  
 Mumma, M. J., Weissman, P. R., & Stern, S. A. 1993, in *Protostars and Planets III*, eds. E. H. Levy, & J. I. Lunine, 1177  
 Mumma, M. J., McLean, I. S., DiSanti, M. A., et al. 2001, *ApJ*, 546, 1183  
 Mumma, M. J., DiSanti, M. A., Dello Russo, N., et al. 2003, *Adv. Space Res.*, 31, 2563  
 Rothman, L. S., Gordon, I. E., Barbe, A., et al. 2009, *J. Quant. Spectr. Radiat. Transf.*, 110, 533  
 Schleicher, D. 2008, *IAU Circ.*, 7342, 1  
 Schleicher, D., & Woodney, L. 2007, *IAU Circ.*, 8903, 1  
 Šimečková, M., Jacquemart, D., Rothman, L. S., Gamache, R. R., & Goldman, A. 2006, *J. Quant. Spectr. Radiat. Transf.*, 98, 130  
 Swings, P. 1941, *Lick Obs. Bull.*, 19, 131  
 Villanueva, G. L., Mumma, M. J., Novak, R. E., & Hewagama, T. 2008, *Icarus*, 195, 34  
 Villanueva, G. L., Mumma, M. J., DiSanti, M. A., et al. 2011a, *Icarus*, 216, 227  
 Villanueva, G. L., Mumma, M. J., & Magee-Sauer, K. 2011b, *J. Geophys. Res.* Pl., 116, E08012  
 Xie, X., & Mumma, M. J. 1992, *ApJ*, 386, 720  
 Xie, X., & Mumma, M. J. 1996, *ApJ*, 464, 442